

Static Analysis of Functionally Graded Piezoelectric Beams Based on Higher-Order Shear Deformation Theory under Thermal Loads

MOSTAFA ABBASI¹, AHAD ARMIN¹, BASHIR BEHJAT¹, MOHAMMAD REZA ESLAMI¹

¹ Distinguished Center of Thermoelasticity, Mechanical Engineering Department, Amirkabir University of Technology, Hafez Ave., Tehran 15914, Iran. e-mail: musan.abbasi@gmail.com

Abstract In this article, static analysis of functionally graded piezoelectric beams based on the higher-order shear deformation theory under thermal loads is investigated. The beam with functionally graded piezoelectric material (FGPM) is graded in the thickness direction with a power law distribution for the piezoelectric material properties. The electric potential is assumed linear across the beam thickness. The governing equations are obtained using the potential energy and the Hamilton's principle. The exact solution of simply supported functionally graded piezoelectric beam is obtained by the finite Fourier transformation. Results are presented for different power law indices under thermal gradient.

Key words functionally graded piezoelectric material, beam, exact solution, static analysis, higher order shear deformation, Fourier transformation

1. Introduction

Piezoelectric actuators and sensors have novel applications for microelectromechanical systems and smart material systems, especially in the medical industries. Since most applications involve operations in changing thermal environments, increased interests in piezothermoelasticity during recent years have addressed thermo-and electromechanical responses. Nowadays, the use of functionally graded materials (FGM) has gained intensive attention especially in extreme high temperature environment and reducing high thermal stresses.

Smart structures or elements made of these so-called FGPMs are usually superior to the conventional sensors, and actuators are often made of the uni-morph, the bi-morph and the multimorph materials. For a piezoelectric laminate with homogeneous material properties in layers, large bending displacements, high stress concentrations, creep at high temperature, and failure from interfacial bonding are usually presented at the layer interfaces under mechanical or electric loading. These effects may lead to lifetime limitations and reliability reduction. To reduce

the drawbacks, piezoelectric materials and structures with functionally graded material properties along the layer-thickness direction have been introduced and fabricated. [1-2].

In the present study, static analysis of functionally graded piezoelectric beam is carried out under thermal loads using the finite Fourier transformation. In addition, the main aim of the study is to evaluate the influence of the grading on the results.

2. Derivation of the Governing Equation

Consider a functionally graded piezoelectric beam as shown in Fig. 1. The material properties change functionally between the upper and lower surfaces across the beam thickness.

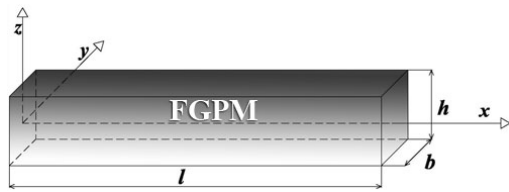


Fig. 1 Schematic diagram of the bar–bar tensile impact apparatus

In the model that is used in this paper, the material properties are expressed as

$$P(z) = P_{ul} \left(\frac{2z+h}{2h} \right)^n + P_l \quad P_{ul} = P_u - P_l \quad (1)$$

where z is the coordinate along the thickness direction of the beam, (P_u, P_l) are the properties of the upper surface and the lower surface, respectively, and h is the thickness of the FGPM beam. The power n is the volume fraction exponent.

In the present analysis, constant surface temperatures are imposed at the upper and lower surfaces. The variation in temperature is assumed to occur along the thickness direction only. Thus, the steady-state heat transfer equation is reduced to a one-dimensional equation as

$$-\frac{d}{dz} \left(K(z) \frac{dT}{dz} \right) = 0. \quad (2)$$

where T is the absolute temperature; T_u and T_l are the applied temperatures on the upper and lower surfaces, respectively, z is the coordinate in the thickness direction, and K is the thermal conductivity, which varies according to the profile given by Eq. 1.

Using the higher-order shear deformation theory, the displacement components are

$$u(x, z) = u_0(x) + z\psi(x) - c_s z^3 (w_{0,x} + \psi), \quad w(x) = w_0(x). \quad (3)$$

where u is the axial displacement, w is the transverse displacement in the z direction, and ψ is the rotation angle of the cross-section with respect to the longitudinal axis. The constant c_s is given by $c_s=4/3h^2$. The subscript zero denotes middle surface and a comma denotes partial differentiation. In terms of the displacement components, the normal and shear strains are given by

$$\varepsilon_x = u_{0,x} + z\psi_{,x} - c_s z^3 (w_{,xx} + \psi_{,x}), \quad \gamma_{xz} = (w_{,x} + \psi) - 3c_s z^2 (w_{,x} + \psi). \quad (4)$$

The constitutive relationships describing the electrical and mechanical interactions for the piezoelectric materials are given as [3]

$$\sigma_{ij} = c_{ijkl}\varepsilon_{kl} - e_{lij}E_l - \beta_{ij}\theta, \quad D_i = e_{ikl}\varepsilon_{kl} + \eta_{il}E_l + p_i\theta. \quad (5)$$

Here, σ_{ij} and ε_{kl} are the stress and strain tensors respectively, D_i is the electrical displacement vector, $E_l = -\varphi_{,l}$ is the electrical field vector, φ is the electrical potential, c_{ijkl} is the elasticity matrix, e_{ikl} is the piezoelectric constant matrix, η_{il} is the dielectrical permittivity coefficient matrix, $\beta_{ij} = c_{ijkl}\alpha_{kl}$ with α_{kl} being the thermal expansion coefficients, p_i denotes the pyroelectric constants, and $\theta = T - T_0$, where T_0 is the reference temperature.

The linear constitutive equations for the stresses and the electric displacements based on the higher-order shear deformation theory reduce to

$$\begin{aligned} \sigma_x &= \hat{E}(z)(u_{0,x} + (z - c_s z^3)\psi_{,x} - c_s z^3 w_{0,xx}) + e_{31}(z)\varphi_{,z} - \hat{E}(z)\alpha(z)\theta, \\ \sigma_{xz} &= \hat{G}(z)(1 - 3c_s z^2)(w_{0,x} + \psi) + e_{15}(z)\varphi_{,x}, \\ D_x &= e_{15}(z)(1 - 3c_s z^2)(w_{0,x} + \psi) - \eta_{11}(z)\varphi_{,x}, \\ D_z &= e_{31}(z)(u_{0,x} + (z - c_s z^3)\psi_{,x} - c_s z^3 w_{0,xx}) - \eta_{33}(z)\varphi_{,z} + p_3(z)\theta. \end{aligned} \quad (6)$$

where \hat{E} and \hat{G} are the Young's modulus and shear modulus, respectively. For mathematical simplification, the potential φ is assumed linear across the FGPM beam thickness as [4]

$$\varphi(x, z) = \frac{z}{h}(\varphi^+(x) - \varphi^-(x)) + \frac{1}{2}(\varphi^+(x) + \varphi^-(x)). \quad (7)$$

where φ^+ and φ^- are the electric potentials on the upper and lower surfaces of the FGPM beam, respectively.

For static analysis of the beam, the virtual work done by the electromechanical internal forces in the FGPM beam is [5]

$$\delta H = \int_V (\sigma_x \delta \varepsilon_x + \sigma_{xz} \delta \gamma_{xz} - D_x \delta E_x - D_z \delta E_z) dv. \quad (8)$$

Using Eqs. 6 and the electric field relations of Eq. 7, and substituting into Eq. 8 and carrying the variational formulation, the dimensionless governing equations are obtained as

$$\begin{aligned}
 a'_1 \bar{u}_{0,\bar{x}\bar{x}} + a'_2 \bar{\psi}_{,\bar{x}\bar{x}} + a'_3 \bar{w}_{0,\bar{x}\bar{x}\bar{x}} + a'_4 \bar{\varphi}_{,\bar{x}}^+ + a'_5 \bar{\varphi}_{,\bar{x}}^- &= 0, \\
 b'_1 \bar{u}_{0,\bar{x}\bar{x}} + b'_2 \bar{\psi}_{,\bar{x}\bar{x}} + b'_3 \bar{\psi}_{,\bar{x}\bar{x}} + b'_4 \bar{w}_{,\bar{x}} + b'_5 \bar{w}_{,\bar{x}\bar{x}\bar{x}} + b'_6 \bar{\varphi}_{,\bar{x}}^+ + b'_7 \bar{\varphi}_{,\bar{x}}^- &= 0, \\
 c'_1 \bar{u}_{0,\bar{x}\bar{x}\bar{x}} + c'_1 \bar{\psi}_{,\bar{x}} + c'_3 \bar{\psi}_{,\bar{x}\bar{x}\bar{x}} + c'_4 \bar{w}_{,\bar{x}\bar{x}} + c'_5 \bar{w}_{,\bar{x}\bar{x}\bar{x}} + c'_6 \bar{\varphi}_{,\bar{x}\bar{x}}^+ + c'_7 \bar{\varphi}_{,\bar{x}\bar{x}}^- &= 0, \\
 d'_1 \bar{u}_{0,\bar{x}} + d'_2 \bar{\psi}_{,\bar{x}} + d'_3 \bar{w}_{,\bar{x}\bar{x}} + d'_4 \bar{\varphi}^+ + d'_5 \bar{\varphi}^- + d'_6 \bar{\varphi}_{,\bar{x}\bar{x}}^+ + d'_7 \bar{\varphi}_{,\bar{x}\bar{x}}^- &= d'_8, \\
 e'_1 \bar{u}_{0,\bar{x}} + e'_2 \bar{\psi}_{,\bar{x}} + e'_3 \bar{w}_{,\bar{x}\bar{x}} + e'_4 \bar{\varphi}^+ + e'_5 \bar{\varphi}^- + e'_6 \bar{\varphi}_{,\bar{x}\bar{x}}^+ + e'_7 \bar{\varphi}_{,\bar{x}\bar{x}}^- &= e'_8.
 \end{aligned} \tag{9}$$

where the dimensionless values are defined as

$$\bar{u}_0 = \frac{u}{l}, \quad \bar{x} = \frac{x}{l}, \quad \bar{w}_0 = \frac{w_0}{l}, \quad \bar{\varphi}^+ = \frac{e_{31u}}{\hat{E}_u l} \varphi^+, \quad \bar{\varphi}^- = \frac{e_{31u}}{\hat{E}_u l} \varphi^-. \tag{10}$$

Here, l is the length of the beam, \hat{E}_u and e_{31u} are the Young's modulus and the piezoelectric constant of the upper surface of the FGPM beam, respectively. The sign (-) indicates dimensionless value.

3. Solution Procedure

In the present analysis, an analytical solution is obtained for the simply supported FGPM beams with the following boundary conditions as

$$\sigma_x = 0 \rightarrow \bar{u}_{,\bar{x}} = \bar{\psi}_{,\bar{x}} = 0, \quad \bar{w} = 0, \quad \bar{\varphi} = 0 \rightarrow \bar{\varphi}^+ = \bar{\varphi}^- = 0 \quad \bar{x} = 0, 1 \tag{11}$$

To solve the system of Eqs. 9, the finite Fourier transformation can be used as

$$\begin{aligned}
 \bar{u}_{0m} &= \int_0^1 \bar{u}_0(\bar{x}) \cos(m\pi\bar{x}) d\bar{x}, \quad \bar{\psi}_m = \int_0^1 \bar{\psi}_0(\bar{x}) \cos(m\pi\bar{x}) d\bar{x}, \\
 \bar{w}_{0m} &= \int_0^1 \bar{w}_0(\bar{x}) \sin(m\pi\bar{x}) d\bar{x}, \\
 \bar{\varphi}_m^+ &= \int_0^1 \bar{\varphi}_m^+(\bar{x}) \sin(m\pi\bar{x}) d\bar{x}, \quad \bar{\varphi}_m^- = \int_0^1 \bar{\varphi}_m^-(\bar{x}) \sin(m\pi\bar{x}) d\bar{x}.
 \end{aligned} \tag{12}$$

Formulas for the inverse of transformation are obtained using the relationship from the theory of Fourier series. To obtain the m th Fourier components of the unknown variables, the system of Eqs. 9 must be solved based on the choice of m as.

$$\begin{aligned}
 -r^2 a'_1 \bar{u}_{0m} - r^2 a'_2 \bar{\psi}_m - r^3 a'_3 \bar{w}_{0m} + r a'_4 \bar{\varphi}_m^+ + r a'_5 \bar{\varphi}_m^- &= 0, \\
 b'_1 \bar{u}_{0m} + (b'_2 - r^2 b'_3) \bar{\psi}_m + (r b'_4 - r^3 b'_5) \bar{w}_{0m} + r b'_6 \bar{\varphi}_m^+ + r b'_7 \bar{\varphi}_m^- &= 0, \\
 r^3 c'_1 \bar{u}_{0m} + (r^3 c'_3 - r c'_2) \bar{\psi}_m + (r^4 c'_5 - r^2 c'_4) \bar{w}_{0m} - r^2 c'_6 \bar{\varphi}_m^+ - r^2 c'_7 \bar{\varphi}_m^- &= 0, \\
 -r d'_1 \bar{u}_{0m} - r d'_2 \bar{\psi}_m - r^2 d'_3 \bar{w}_{0m} + (d'_4 - r^2 d'_6) \bar{\varphi}_m^+ + (d'_5 - r^2 d'_7) \bar{\varphi}_m^- &= \frac{2}{r} d'_8, \\
 -r e'_1 \bar{u}_{0m} - r e'_2 \bar{\psi}_m - r^2 e'_3 \bar{w}_{0m} + (e'_4 - r^2 e'_6) \bar{\varphi}_m^+ + (e'_5 - r^2 e'_7) \bar{\varphi}_m^- &= \frac{2}{r}
 \end{aligned} \tag{13}$$

4. Results and Discussion

An FGPM beam of length 0.2m and height 0.0025m with simply supported boundary conditions is assumed. The bottom surface of the FGPM beam is Platinum with the temperature $T=300\text{K}$, whereas the top surface of the beam is PZT-4A with temperature $T=400\text{K}$. It is assumed that the reference temperature is $T_0=293\text{K}$. The material properties of PZT-4 and Platinum are shown in Table 1.

Table 1 Material properties of PZT-4 and Platinum

Material	$\hat{E}(\text{GPa})$	$K(\text{W}/\text{m}^2\text{K})$	$\alpha(1/^\circ\text{K})$	$e_{31}(\text{C}/\text{m}^2)$	$e_{15}(\text{C}/\text{m}^2)$	$\eta_{11}(\text{N}/\text{m}^2)$	$\eta_{33}(\text{N}/\text{m}^2)$	$p_3(\text{C}/^\circ\text{K}\text{m}^2)$
PZT-4	74	9	4.4×10^{-6}	-0.9	4.6	8.26×10^{-11}	9.03×10^{-11}	3×10^{-6}
Platinum	168	77.8	9×10^{-6}	0	0	0	0	0

The FGPM beam is studied under a thermal gradient through its thickness direction. The temperature of the top PZT-4-rich surface is fixed at 400°K and that of the bottom Platinum surface is kept constant at 300°K . It is assumed that the reference temperature is $T_0=295^\circ\text{K}$. The temperature field through the thickness of the beam is shown in Fig. 2.

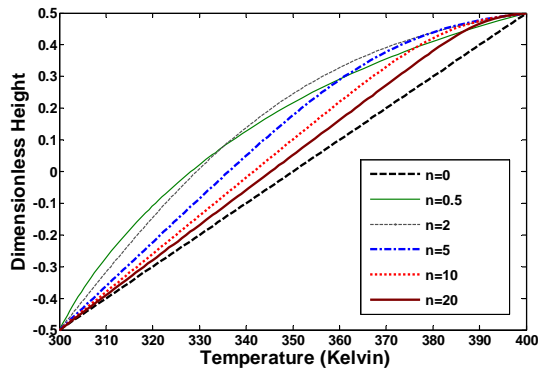


Fig. 2 Distribution of the temperature across the dimensionless thickness of the FGPM beam.

The dimensionless deflection through the dimensionless beam length is shown in Fig. 3 for various volume fraction exponents n . It is observed that for different values of n , different deflection profiles for the beam under thermal gradient is obtained. Figure 4 depicts the upper surface axial stress σ_x of the FGPM simply supported beam ($x=0.25l$) versus volume fraction indexes under thermal gradient. Figure 5 shows the distribution of shear σ_{xz} across the thickness direction at $x=0.25L$ for the FGPM beam under thermal gradient. Also, Figure 6 shows the electric displacements D_x across the thickness direction for the FGPM beam caused by thermal load. It is observed that the electric displacements change slightly for different power law indices under thermal load.

5. Conclusion

In the present paper, the effect of thermal loads on the static behavior of a functionally graded

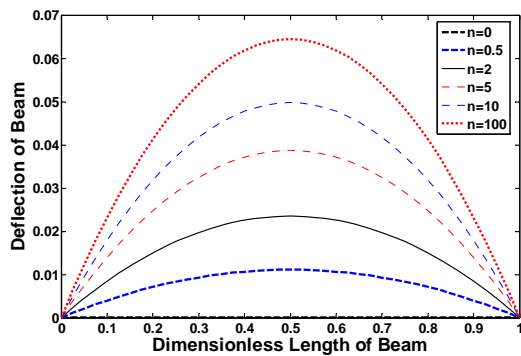


Fig. 3 Distribution of dimensionless deflection through the dimensionless length.

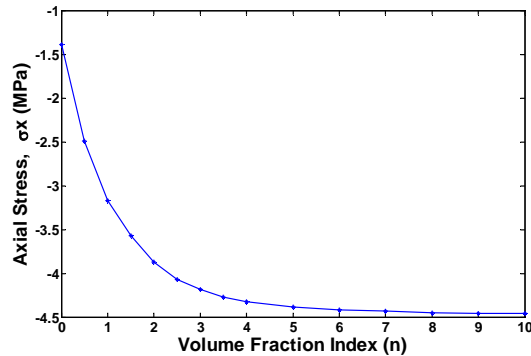


Fig. 4 The upper surface axial stress σ_x versus volume fraction index.

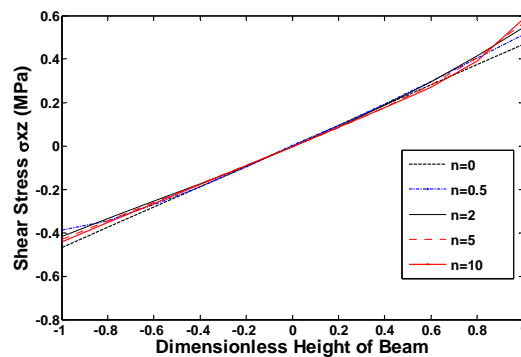


Fig. 5 Distribution of dimensionless shear stress across the dimensionless height.

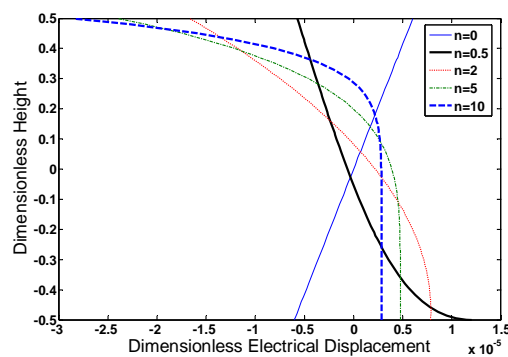


Fig. 6 Distribution of dimensionless electric displacement across the dimensionless height.

piezoelectric beam is investigated using the higher-shear deformation theory. The solution of governing equations is obtained using the virtual work and the finite Fourier transformation. Results show the displacement and stress components change significantly and gradually unlike the electric potential field for different power law indices. Moreover, it can be said that for the intermediate values of n the electric potential field is maximum.

Reference

1. Takagi, K., Li, J.F., Yokoyama, S., Watanabe, R.: Fabrication and evaluation of PZT/Pt piezoelectric composites and functionally graded actuators. *J Eur. Ceram. Soc.* 23, 1577-1586 (2003)
2. Wu, X.H., Chen, C.Q., Shen, Y.P., Tian, X.G.: A high order theory for functionally graded Piezoelectric shells. *Int. J. Solids Struct.* 39, 5325-5344 (2002)
3. Wang, B.L., and Noda, N.: Design of a smart functionally graded Thermo piezoelectric composite structure. *Smart Mater. and Struct.* 10, 189-193 (2001)
4. Kapuria, S., Ahmed, A. and Dumir, P.C.: Coupled consistent third-order theory for hybrid piezoelectric beams under thermal load. *J. Therm. Stresses* 27, 405-424 (2004)
5. Trindade, M.A. and Benjeddou, A.: On higher-order modeling of smart beams with embedded shear-mode piezoceramic actuators and sensors. *Mech. Adv. Mater. Struct.* 13(5), 357-369 (2006)